PERGAMON

International Journal of Solids and Structures 37 (2000) 7307–7327

INTERNATIONAL JOURNAL OF SOLIDS and STRUCTURES

www.elsevier.com/locate/ijsolstr

Simulation of mode I crack growth in polymers by crazing

M.G.A. Tijssens [a,*], E. van der Giessen [b], L.J. Sluys [a]

[a] *Delft University of Technology, Koiter Institute Delft, Stevinweg 1, 2628 CN Delft, Netherlands*
[b] *Delft University of Technology, Koiter Institute Delft, Mekelweg 2, 2628 CD Delft, Netherlands*

Received 16 August 1999; in revised form 15 February 2000

Abstract

Crazing in amorphous polymers under mode I loading conditions is simulated using the concept of embedded cohesive surfaces with a recently proposed model. The dependence of the predicted crack growth resistance on the crazing material parameters is studied. In general, for constant loading rate, a lower fracture toughness is predicted for shorter craze lengths. However, since the widening of the craze is of a viscoplastic nature, this trend can be reversed for increasing loading rate. The parameter variations indicate that the perfectly plastic Dugdale cohesive zone model is not applicable to crazing. Mesh sensitivity with respect to length and orientation of the cohesive surface elements is also studied. Convergence of crack growth resistance and crack path predictions can only be expected for very fine, randomly oriented meshes. © 2000 Published by Elsevier Science Ltd.

Keywords: Finite element analysis; Crazing; Cohesive surfaces

1. Introduction

Amorphous glassy polymers, such as polystyrene and PMMA, fail due to crazing. Crazing starts with the nucleation of microvoids in regions of stress concentrations and is primarily normal to the maximum principal stress. These voids do not coalesce to form cracks, but highly stretched molecular chains or fibrils stabilize this process to create a crack-like feature bridged by fibrils: a craze. However, after further craze widening, fibrils break down and a microcrack is formed.

Depending on the type of polymer, the stress state, loading rate, temperature etc., the ultimate fracture occurs by the propagation of crazing and cracking, or by the linking-up of large numbers of microcracks. In the first case, one observes a macroscopically flat fracture surface. Multiple crazes and cracks are very typical in many blends of amorphous polymer toughened by rubber particles. Again, depending on the material and conditions, the bulk material can remain elastic during crazing or may take place in competition with plastic flow (or shear yielding). In fact, the latter competition will control the transition between brittle and ductile fractures in polymer–rubber blends.

Various attempts have been made to model the crazing process at different length scales (Brown, 1991; Xiao and Curtin, 1995; Hui et al., 1992). However, there is a large gap in length scale between detailed

* Corresponding author. Tel.: +31-15-278-6602; fax: +31-15-278-6383.
E-mail address: m.g.a.tijssens@wbmt.tudelft.nl (M.G.A. Tijssens).

0020-7683/00/$ - see front matter © 2000 Published by Elsevier Science Ltd.
PII: S0020-7683(00)00200-6

studies on the crazing process itself and the role of crazing in polymer fracture. To understand the role of crazing during failure of polymers, a new cohesive surface model for crazing has been developed by Tijssens et al. (2000). This model aims at a description of crazing at a characteristic length scale of several microns such that the simulation of failure of polymers or blends becomes feasible. The cohesive surface model captures the essential features of crazing within an effective traction–separation law spanning the total lifetime of a craze, i.e., from initiation of a craze nucleus until breakdown of the fibrillated polymer material.

This cohesive surface model has been employed by Estevez et al. (2000) for the first study of the interaction between plastic flow and crazing. They used a single cohesive surface in front of an initially blunt crack under mode I conditions. Crack deflection and crack bridging are excluded in such a model. As mentioned above, there is a large class of fracture situations which do involve multiple or even high densities of crazes. Using the concept of embedded cohesive surfaces, as pioneered by Xu and Needleman (1994), crazing can be simulated without a priori assuming a predetermined craze path.

In this paper, we adopt this idea and embed cohesive surface elements for crazing in a standard finite element discretization of the continuum representing the bulk polymer. This methodology is applied to study how an existing sharp crack propagates by crazing. Thus, failure can potentially occur along the edges of continuum elements, and the final crack can find its own path without criteria other than in the cohesive surface law. The dependence of the predicted crack growth resistance on the material parameters in the craze model is studied. Due attention is also given to the sensitivity of the predictions to mesh density and orientation.

2. Material model

This section briefly reviews the model presented in Tijssens et al. (2000) wherein detailed information on the cohesive surface model can be found.

2.1. Cohesive surface idealization for crazes

Crazes in amorphous polymers generally reach lengths in the order of tenths of millimeters, whereas the width (or thickness) of the craze remains in the order of several micrometers. Neglecting its thickness, Tijssens et al. (2000) replaced a craze by a cohesive surface, as illustrated in Fig. 1. The separation between two initially adjacent material points, one situated in the upper bulk–craze interface and the other in the bottom bulk–craze interface is described by a separation vector $\boldsymbol{\Delta}$ with normal component Δ_n and tangential component Δ_t with respect to the midplane of the cohesive surface. The traction vector $\boldsymbol{T}$ is energetically conjugate to $\boldsymbol{\Delta}$ and has components T_n and T_t. The properties of the craze matter are captured in a traction–separation law, which will be specified below.

The crazing process is described with three separate stages: (i) the initiation of a craze, (ii) subsequent widening of the fibrils and (iii) final breakdown of the fibrillar material. A typical traction–separation law for a craze is shown in Fig. 2. Initiation of a craze is taken based on the stress-state dependent criterion proposed by Sternstein et al. (1968). In this particular criterion, the cohesive surface normal traction T_n and the hydrostatic stress σ_m are both responsible for the initiation of a craze, according to

$$f(T_n, \sigma_m) = \frac{3}{2}\sigma_m - \frac{1}{2}A + \frac{B}{6\sigma_m} - T_n \tag{1}$$

in which A and B are temperature dependent constants. Starting from an unstressed state, $f(T_n, \sigma_m)$ remains positive until the state of stress is such that $f(T_n, \sigma_m) = 0$. At this instant, a craze is initiated. Stress states for which $f(T_n, \sigma_m) < 0$ cannot be reached without triggering crazing. After craze initiation, Eq. (1) becomes meaningless.

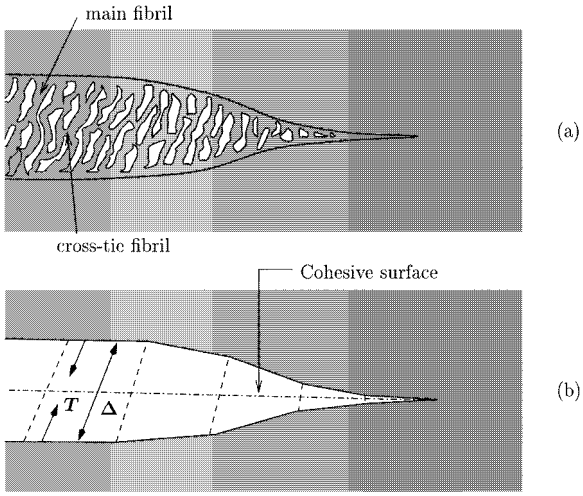

Fig. 1. Schematic of modeling a craze (a) by a cohesive surface (b) characterized by a traction $\boldsymbol{T}$ and a separation $\boldsymbol{\Delta}$ over this surface.

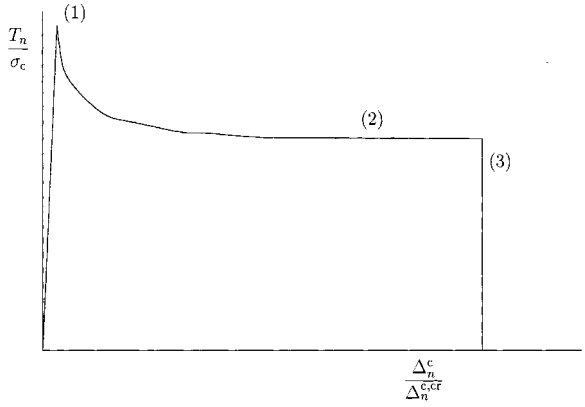

Fig. 2. Schematic of the traction–separation law for a craze. The numbers indicate (1) craze initiation followed by softening, (2) rate dependent surface drawing stress and (3) final breakdown.

Once a craze is initiated, widening of the craze is assumed to be a process of drawing in new polymer material from the craze–bulk interface (Kramer, 1983; Kramer and Berger, 1990). This is illustrated schematically in Fig. 3. Motivated by the early qualitative analysis of Kramer and Berger (1990) and of Leonov and Brown (1992) and partly by the numerical results of the more quantitative study in Van der Giessen and Lai (1997), Tijssens et al. (2000) proposed a rather phenomenological constitutive description of craze widening in which the normal separation rate $\dot{\Delta}_{\mathrm{n}}^{\mathrm{c}}$ as a function of the normal stress T_{n} is given by

$$\dot{\Delta}_{\mathrm{n}}^{\mathrm{c}} = \dot{\Delta}_0 \exp\left[-\frac{A^*\sigma_{\mathrm{c}}}{T}\left(1-\frac{T_{\mathrm{n}}}{\sigma_{\mathrm{c}}}\right)\right]. \tag{2}$$

Here, A^*, $\dot{\Delta}_0$, and σ_{c} are material constants; $\dot{\Delta}_0$ is a reference separation rate (which is attained when T_{n} reaches values as high as σ_{c}); A^* governs a linear drop in normal traction T_{n} with temperature T at a given separation rate $\dot{\Delta}_{\mathrm{n}}^{\mathrm{c}}$ and σ_{c} is the athermal stress for craze widening.

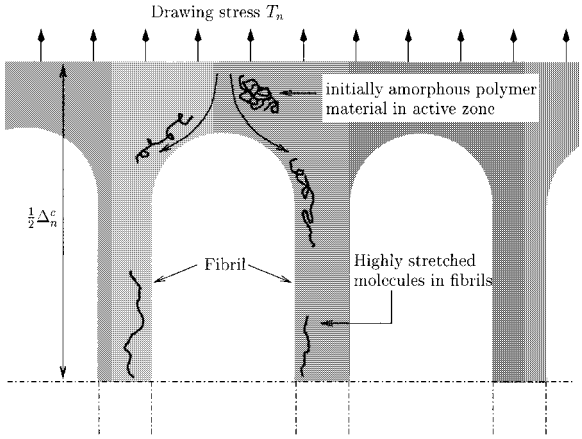

Fig. 3. Illustration of the surface drawing mechanism.

The material inside a craze has a complex structure in which long cylindrical fibrils of polymer material are interconnected by cross-tie fibrils which give the craze some tangential load carrying capacity while it widens. In a cohesive surface representation, we account for a resistance against tangential separation in terms of a constitutive description of $\dot{\Delta}_t^c$ as a function of T_t. Because the geometry of the craze material suggests a coupling between the tangential separation and the normal separation model, Tijssens et al. (2000) proposed the following viscoplastic tangential separation law similar to Eq. (2):

$$\dot{\Delta}_t^c = \dot{\Gamma}_0 \left\{ \exp\left[-\frac{A^* \tau_c}{T}\left(1 - \frac{T_t}{\tau_c}\right)\right] - \exp\left[-\frac{A^* \tau_c}{T}\left(1 + \frac{T_t}{\tau_c}\right)\right]\right\} \tag{3}$$

in which $\dot{\Gamma}_0$ and τ_c are material parameters. Note that in contrast to the normal viscoplastic widening law (2), an extra term is included which ensures that $\dot{\Delta}_t^c$ is an odd function of T_t. To limit the number of material parameters, we follow Tijssens et al. (2000) and use $\dot{\Gamma}_0 = \sqrt{3}\dot{\Delta}_0$ and $\tau_c = \sigma_c/\sqrt{3}$.

Although the precise mechanism that governs craze breakdown is still not known, transmission electron microscopy (TEM) observations of craze breakdown (Kramer and Berger, 1990) show that upon breakdown, a pear-shaped void initiates at the craze–bulk interface which gradually grows in size upon further increasing the width of the craze. In a cohesive surface model, it is not known a priori how fast such a void expands nor is it known what its initial size is. This is inevitably related to the size of the imperfections and the molecular weight of the polymer. Recently, important theoretical progress has been made in understanding the kinetics of craze breakdown. Brown (1991) was the first to point out the important role of the cross-tie fibrils, followed by more detailed models of Hui et al. (1992) and Sha et al. (1997). However, the theoretical knowledge regarding craze breakdown is far from complete and still much further research seems necessary to arrive at a satisfactory description of craze breakdown kinetics on the length scale that we are aiming for in our cohesive surface description. We therefore follow the experimental results of Döll et al. (1979) from which it is concluded that craze breakdown occurs as soon as the plastic craze opening Δ_n^c reaches a critical value $\Delta_n^{c,cr}$ which is taken to be constant with respect to time, temperature and loading rate.

2.2. Numerical implementation

Following Tijssens et al. (2000), we account for finite strains in the continuum description, using a total Lagrangian description. The numerical solution of the equilibrium equations is obtained using a linear

incremental analysis within the finite element context. For each discrete time step Δt during the incremental procedure, equilibrium is specified through the rate form of the principle of virtual work:

$$\Delta t \int_V (\dot{\tau}^{ij}\delta\eta_{ij} + \tau^{ik}\dot{u}^j_{,k}\delta u_{j,i})\,\mathrm{d}V + \Delta t \int_{S_i} \dot{T}_\alpha \delta \Delta_\alpha \,\mathrm{d}S = \Delta t \int_{S_u} \dot{t}^i \delta u_i \,\mathrm{d}S - \left[\int_V \tau^{ij}\delta\eta_{ij}\,\mathrm{d}V + \int_{S_i} T_\alpha \delta\Delta_\alpha \,\mathrm{d}S - \int_{S_u} t^i \delta u_i \,\mathrm{d}S \right] \tag{4}$$

in which V and S_u are the volume and outer surface of the body in the reference configuration, respectively, and S_i is the current internal cohesive surface. The latter is the collection of all cohesive surfaces contained in V. Here, V is discretized by linear triangular elements, and cohesive surface elements may be introduced essentially in between all adjacent elements (but for practical reasons confined to a subregion of V). The term in Eq. (4) between square brackets is the equilibrium correction which is zero for a state of perfect equilibrium. This term is included to prevent drifting of the solution from the true equilibrium path due to the finite time increments.

Inelastic deformation of the polymer is assumed to be limited here to crazing, which is concentrated in the cohesive surfaces. The bulk is isotropic and linear elastic with elastic strains remaining small. For computational convenience, this is implemented in terms of the relation,

$$\dot{\tau}^{ij} = L^{ijkl}\dot{\eta}_{kl} \tag{5}$$

between the second Piola–Kirchhoff stress $\boldsymbol{\tau} = \tau^{ij}\boldsymbol{e}_i\boldsymbol{e}_j$ and the Lagrangian strain $\boldsymbol{\eta} = \eta_{ij}\boldsymbol{e}^i\boldsymbol{e}^j$, with the elastic moduli L^{ijkl} for an isotropic elastic material being expressed in terms of Young's modulus E and Poisson's ratio v.

In the previous section, the constitutive description of crazes has been phrased in terms of the rate equations (2) and (3) for the normal and tangential components $(\dot{\Delta}^{\mathrm{c}}_{\mathrm{n}}, \dot{\Delta}^{\mathrm{c}}_{\mathrm{t}})$ of the separation vector $\boldsymbol{\Delta}^{\mathrm{c}}$. The constitutive description of the cohesive surfaces is completed by

$$\dot{T}_\alpha = k^*_\alpha(\dot{\Delta}_\alpha - \dot{\Delta}^{\mathrm{c}}_\alpha), \quad \alpha = n, t \tag{6}$$

in which we employ a forward gradient scheme (Peirce et al., 1984) in order to improve the numerical stability (Tijssens et al., 2000). The stiffness k^*_α is defined by

$$k^*_\alpha = k_\alpha \Big/ \left(1 + k_\alpha \theta \frac{\partial \dot{\Delta}^{\mathrm{c}}_\alpha}{\partial T_\alpha}\Delta t\right), \quad \alpha = n, t \tag{7}$$

in which k_α is the normal or tangential stiffness of the cohesive surface and Δt is the time increment. For the numerical analysis in this paper, we have used $\theta = 0.5$.

The finite element equations are obtained by eliminating the stress rates $\dot{\tau}^{ij}$ using Eq. (5) and eliminating the cohesive surface traction rates using Eqs. (2), (3) and (6). As pointed out by Schellekens and De Borst (1993), the numerical integration of the stiffness contributions of the cohesive surface elements with Gauss quadrature may lead to numerical errors if traction gradients are large. In such cases, the numerical integration is best carried out with Newton–Cotes integration, which is the scheme adopted in this paper.

Prior to craze initiation, the plastic widening rate of the craze vanishes ($\dot{\Delta}^{\mathrm{c}}_\alpha = 0$) and the stiffness k_α is artificial. Its value needs to be high so that the elastic deformation in the cohesive surfaces does not significantly contribute to the overall elastic properties. Once crazing is initiated, the stiffness k_α reflects the instantaneous elastic properties of the craze fibrils and part of the active material in the craze (Fig. 1). For this reason, Estevez et al. (2000) proposed an evolution of the cohesive surface stiffness based on the extension of the craze fibrils. In this paper, we simply treat the stiffness k_{n} as a constant during the entire crazing process.

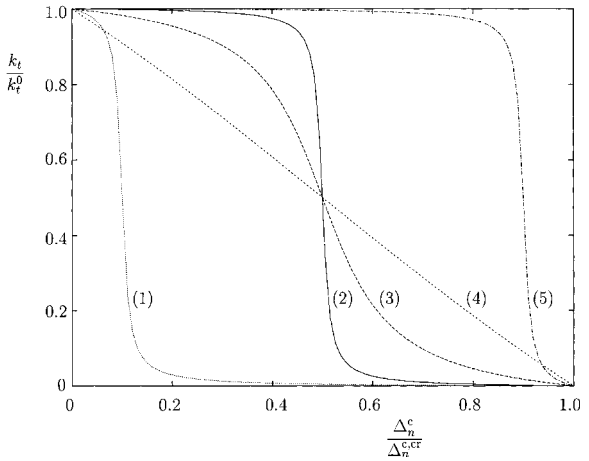

Fig. 4. Illustration of the decrease of tangential cohesive surface stiffness with increasing craze widening for various values of c_1 and c_2 from Eq. (8): (1) $c_1 = 100$, $c_2 = 0.1$, (2) $c_1 = 100$, $c_2 = 0.5$, (3) $c_1 = 10$, $c_2 = 0.5$, (4) $c_1 = 1$, $c_2 = 0.5$, (5) $c_1 = 100$, $c_2 = 0.9$.

Although initially k_t must be sufficiently large for reasons mentioned above, after substantial widening, the craze matter exhibits a low but finite tangential stiffness due to the cross-tie fibrils. Tijssens et al. (2000) proposed an exponentially decaying relation for the tangential stiffness. However, it may be argued that the main fibrils of the craze, immediately after craze initiation, are still quite capable of resisting tangential deformation. The tangential stiffness may then drop down only after a certain amount of craze widening has occurred. Here, we therefore adopt another decaying law in which the tangential stiffness evolves with the craze width Δ_n^c according to

$$k_t = k_t^0 \frac{\arctan[c_1(\Delta_n^c/\Delta_n^{c,cr} - c_2)] - \arctan[c_1(1 - c_2)]}{\arctan[-c_1 c_2] - \arctan[c_1(1 - c_2)]}. \tag{8}$$

This is illustrated in Fig. 4. The influence of the constants c_1 and c_2 will be studied later.

As mentioned above, the forward gradient-based relation (6) is used for the overall stiffness matrix. Rather than using this for $\alpha = n$ also to compute the incremental normal traction, $\Delta T_n = \dot{T}_n \Delta t$, we use the exact solution for the increment of the normal traction, which is obtained by substituting Eq. (2) into Eq. (6). Integrating the resulting equation over the time interval $[t, t + \Delta t]$ and invoking that the normal separation rate $\dot{\Delta}_n^c$ is constant over this interval, we obtain

$$\Delta T_n = -\frac{T}{A} \ln \left\{ \left(1 - \frac{\dot{\Delta}_0}{\dot{\Delta}_n} \exp\left[-\frac{A}{T}(\sigma_c - T_n) \right] \right) \exp\left[-\frac{A}{T} k_n \dot{\Delta}_n \Delta t \right] + \frac{\dot{\Delta}_0}{\dot{\Delta}_n} \exp\left[-\frac{A}{T}(\sigma_c - T_n) \right] \right\}. \tag{9}$$

The increased accuracy of the cohesive traction updating obtained by using this increment was found to be necessary right during the first stages of craze widening. Since the tangential separation is expected to remain relatively small and the exact solution is computationally expensive, we use the forward gradient updating for the tangential separation mode ($\alpha = t$) according to Eq. (6).

3. Problem formulation

From experiments, it is known that crazes tend to propagate perpendicular to the direction of maximum principle stress. In view of this, we now focus on mode I crack tip conditions to study the numerical aspects

of the cohesive surface methodology and the physical aspects of the cohesive surface model for crazing. Assuming that the length of the active, i.e., not broken down, craze remains smaller than the length of the existing crack and any other dimensions, we adopt the boundary layer approach for the mode I plane strain fields near the crack tip. Crazing is assumed to be restricted to a circular region of radius R^c in front of the initial crack tip, the so-called process window.

The remote region is taken to be bounded by a circular arc of radius R with $R/R^c = 100$. For this ratio, it has been verified that moving the origin of the mode I crack tip field along with the current crack tip does not significantly alter the results for crack growth resistance. Along the outer arc, the mode I elastic field at a stress intensity factor (SIF) K_I is prescribed via the Cartesian displacement components u_1 and u_2, according to

$$u_1 = K_I \frac{2(1+\nu)}{E}\sqrt{\frac{r}{2\pi}}\cos\frac{1}{2}\theta\left(1 - 2\nu + \sin^2\frac{1}{2}\theta\right), \tag{10}$$

$$u_2 = K_I \frac{2(1+\nu)}{E}\sqrt{\frac{r}{2\pi}}\sin\frac{1}{2}\theta\left(2 - 2\nu - \cos^2\frac{1}{2}\theta\right), \tag{11}$$

where r and θ are polar coordinates with the original crack tip at the origin. Traction-free boundary conditions are imposed along the crack faces.

The finite element mesh is shown in Fig. 5a. To explore the capabilities of the cohesive surface formulation for crazing and possible mesh effects, we do not use the symmetry of the problem so that we can analyze asymmetrically discretized configurations. The process window, i.e., the region in which crazing can occur, is shown in Fig. 5b. In this region, each side of the triangular elements is connected to a cohesive surface as illustrated in Fig. 6.

4. Parameter study

This section deals with the variation of material parameters in the model. We will focus on the parameters related to craze widening and breakdown as the influence of the craze initiation parameters has already been explored in Tijssens et al. (2000) and Estevez et al. (2000). The material parameters are grouped into the following three dimensionless parameters:

$$\frac{A^*\sigma_c}{T}, \quad \frac{\dot{K}_I^2 \Delta_n^{c,cr}}{\dot{\Delta}_0^2 \sigma_c^2}, \quad \frac{E}{\sigma_c}. \tag{12}$$

In all calculations, we have used the material parameters given in Table 1, unless stated otherwise.

To investigate the influence of the dimensionless parameters, crazing and crack growth is confined to the surface ahead of the crack, as in Estevez et al. (2000). In this way, possible mesh effects due to meandering or craze branching do not obscure the results; these will be investigated separately in the subsequent section. Also, we can then make a simple comparison with a Dugdale-like model for a craze, as has been often used in the polymer community (e.g., Döll et al., 1980). For a Dugdale-like cohesive zone (Dugdale, 1960) characterized by "perfectly plastic" behavior with a yield stress σ_c and maximum separation $\Delta_n^{c,cr}$, we can estimate the steady state value of the mode I SIF, K_D^{ss}. Equating the far-field energy release rate $\mathcal{G} = K_D^{ss2}/E$ to the energy needed to break a unit length of the idealized craze, $\Gamma = \sigma_c \Delta_n^{c,cr}$, we obtain

$$K_D^{ss} = \left(\sigma_c \Delta_n^{c,cr} E\right)^{1/2}. \tag{13}$$

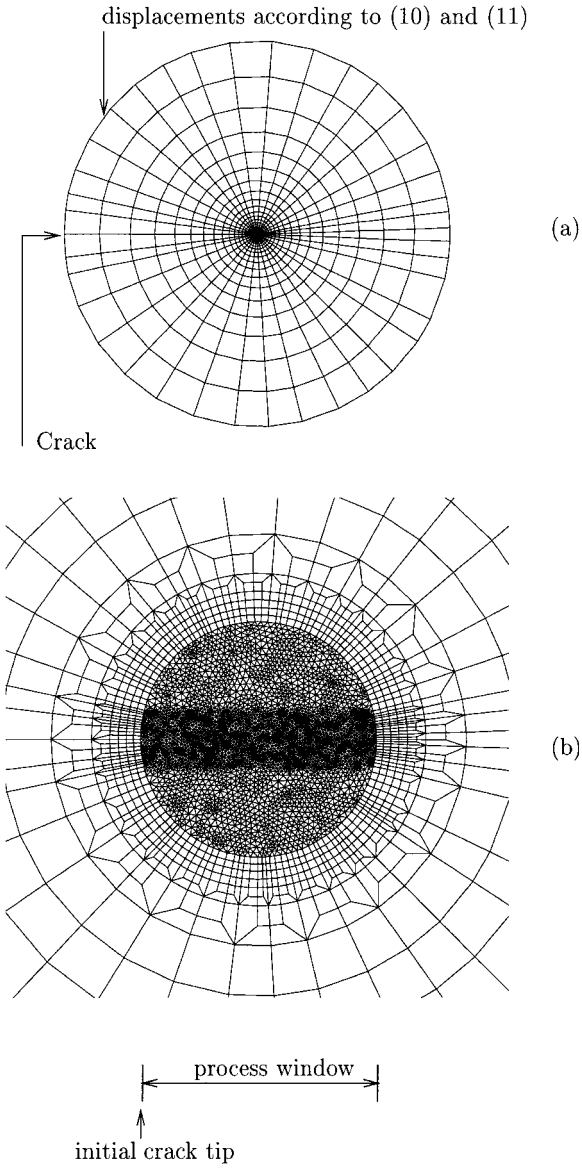

Fig. 5. Example of (a) the global mesh and (b) the unstructured process window used during the calculations.

The "plastic zone size", i.e., the craze length, is estimated through the well-known relation

$$c_{\mathrm{D}} = \frac{\pi}{8}\left(\frac{K_{\mathrm{D}}^{\mathrm{ss}}}{\sigma_{\mathrm{c}}}\right)^2. \tag{14}$$

For the default parameter values given in Table 1, we obtain $K_{\mathrm{D}}^{\mathrm{ss}} = 16.2$ MPa mm$^{1/2}$ and $c_{\mathrm{D}} \approx 0.11$ mm. The estimates $K_{\mathrm{D}}^{\mathrm{ss}}$ and c_{D} are used to normalize K_{I} and the total crack extension Δa in our simulations. The new crack tip position a is defined as the horizontal location of the rightmost cohesive surface integration point (Fig. 5b) for which full craze breakdown has occurred.

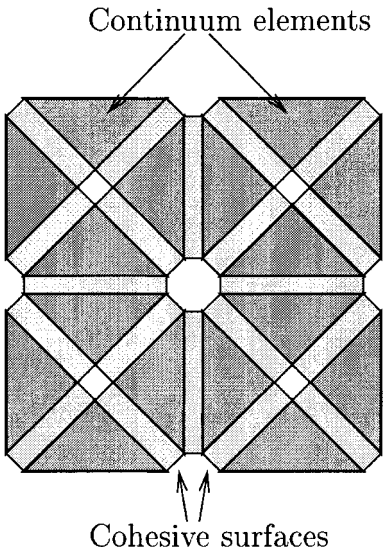

Fig. 6. Configuration of continuum elements with cohesive surfaces.

4.1. Parameter 1, $A^*\sigma_c/T$

The first parameter describes the linear temperature dependence of the polymer. Variation of this parameter is obtained by varying A^* in the calculations. Besides the default value in Table 1, A^* takes the values 48.83, 195.3 and 1006 K/MPa. Variations in temperature are not considered here since that would also influence the stress level at which crazing initiates, as shown in Tijssens et al. (2000). The loading rate is given by $\dot{K}_I = 1.0\ \text{MPa mm}^{1/2}\,\text{s}^{-1}$. The crack growth curves, K_I vs Δa, predicted for various values of $A^*\sigma_c/T$ are given in Fig. 7.

Since σ_c is the athermal drawing stress of the craze, decreasing $A^*\sigma_c/T$ effectively results in a decrease of the drawing stress T_n during craze widening due to the more viscous nature of the drawing process. Since the stress level at which the craze initiates is not affected by A^*, this implies that for relatively low values of $A^*\sigma_c/T$, the surrounding bulk is unloaded faster, and therefore, the redistribution of stresses occurs faster during the craze widening process. Consequently, the craze tip propagation speed increases for decreasing $A^*\sigma_c/T$.

According to Eq. (2), decreasing $A^*\sigma_c/T$ for constant drawing stress $T_n < \sigma_c$ results in an increasing widening rate $\dot{\Delta}_n^c$. The fibrillar material will therefore tend to break down earlier. From Fig. 7, it is seen that decreasing $A^*\sigma_c/T$ results in a lower SIF K_I^0 for crack growth initiation. However, the outcome of the

Table 1
Default material parameters used during all calculations

E	(MPa)	3240
v		0.35
σ_c	(MPa)	30
$\dot{\Delta}_0$	(mm/s)	1.0×10^{-2}
$\Delta_n^{c,cr}$	(mm)	2.7×10^{-3}
A^*	(K/MPa)	100.6
A	(MPa)	12
B	(MPa^2)	5046

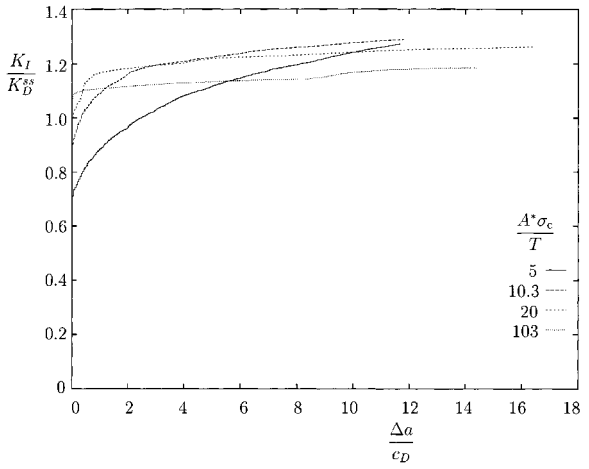

Fig. 7. Crack growth resistance curves for variation of $A^*\sigma_c/T$.

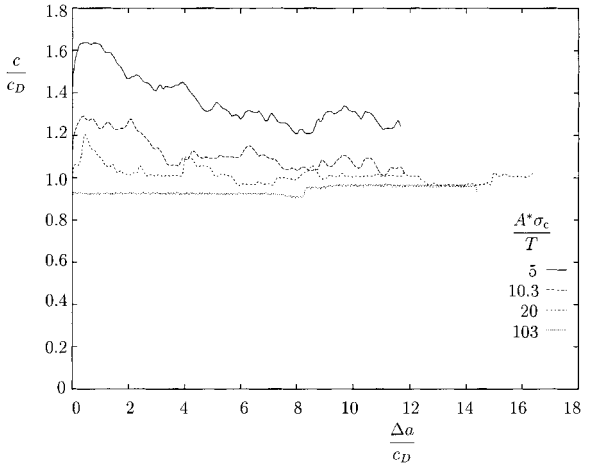

Fig. 8. Development of craze length c/c_D as a function of crack length $\Delta a/c_D$ for various values of $A^*\sigma_c/T$.

numerical analysis is a result of the competition between craze initiation, widening of already existing crazes and unloading of the surrounding bulk. As a consequence of this competition, the lower drawing stress T_n for lower values of $A^*\sigma_c/T$ is accompanied by an increasing craze tip propagation speed, which results in a larger craze length c, as shown in Fig. 8. This results in a higher load carrying capacity of the craze and hence a larger steady state value of the mode I SIF with decreasing $A^*\sigma_c/T$, as observed in Fig. 7. The larger K_I^{ss} as a result of a larger c is consistent with the rate-independent Dugdale estimate in Eqs. (13) and (14). However, the lowering of the crack growth initiation SIF K_I^0 cannot be predicted by the Dugdale model.

4.2. Parameter 2, $K_I^2\Delta_n^{c,cr}/\Delta_0^2\sigma_c^2$

This parameter relates the rate of loading to the rate at which craze widening takes place. Variation of this parameter is obtained by varying the loading rate $\dot{K}_I$ in the calculations. The values used for $\dot{K}_I$ are 0.1,

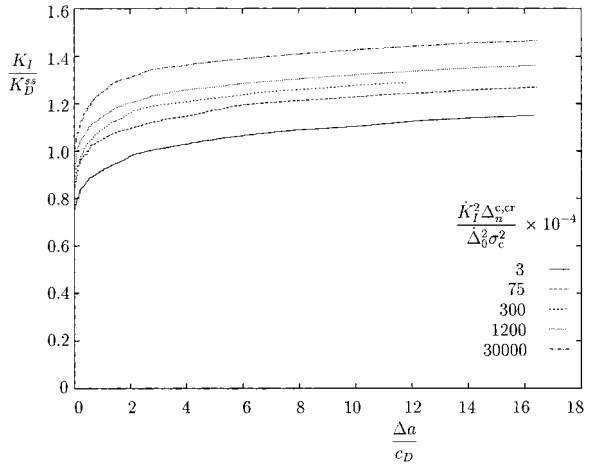

Fig. 9. Crack growth resistance curves for variation of $\dot{K}_I^2 \Delta_n^{c,cr} / \dot{\Delta}_0^2 \sigma_c^2$ through $\dot{K}_I$.

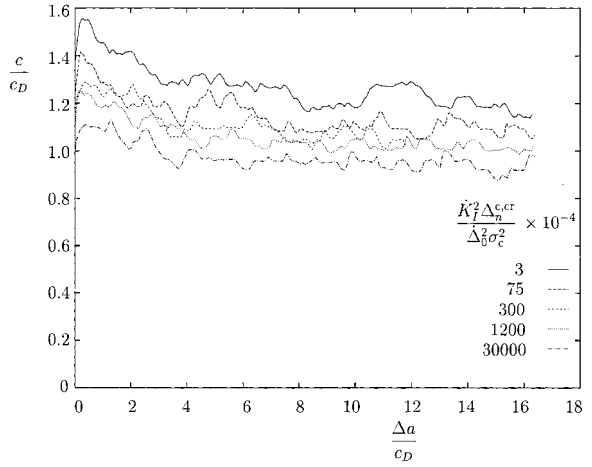

Fig. 10. Development of craze length c/c_D as a function of crack length $\Delta a/c_D$ for various values of $\dot{K}_I^2 \Delta_n^{c,cr} / \dot{\Delta}_0^2 \sigma_c^2$.

0.5, 1, 2 and 10 MPa $mm^{1/2} s^{-1}$. From Fig. 9, we observe that a higher value of $\dot{K}_I^2 \Delta_n^{c,cr} / \dot{\Delta}_0^2 \sigma_c^2$ results in a higher steady state value of the mode I SIF. The shape of the resistance curves is hardly affected by the value of $\dot{K}_I^2 \Delta_n^{c,cr} / \dot{\Delta}_0^2 \sigma_c^2$.

The higher value of $\dot{K}_I$ relative to the viscoplastic widening rate of the craze results in a higher drawing stress T_n of the craze. This can also be interpreted as effectively increasing the "yield stress" in the Dugdale model. The slower redistribution of stresses in the continuum that is a consequence of the higher drawing stress results in a lower craze tip propagation speed. At the same time, the higher plastic separation rate $\dot{\Delta}_n^c$ results in a shorter lifetime of the fibrils.

Both the lower craze propagation speed and higher plastic separation rate $\dot{\Delta}_n^c$ result in a smaller craze length c (Fig. 10). The classical Dugdale model is rate independent and would therefore reveal the

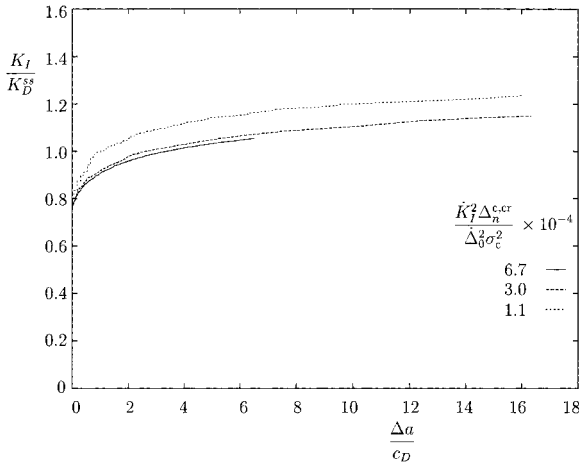

Fig. 11. Crack growth resistance curves for variation of $\dot{K}_{\mathrm{I}}^2 \Delta_{\mathrm{n}}^{\mathrm{c,cr}} / \dot{\Delta}_0^2 \sigma_{\mathrm{c}}^2$ through $\Delta_{\mathrm{n}}^{\mathrm{c,cr}}$.

opposite trend, i.e., a decrease in $K_{\mathrm{D}}^{\mathrm{ss}}$ with decreasing c_{D} (Eq. (14)). For high values of $A^* \sigma_{\mathrm{c}} / T$, loading rate effects are less important. This is because the separation process then tends to become perfectly plastic, as can be seen from Eq. (2). While varying the loading rate $\dot{K}_{\mathrm{I}}$ for the default parameters given in Table 1, the influence of the viscoplastic behavior of the craze widening process is important. It is the viscoplastic nature of craze widening which results in an increase of the steady state value $K_{\mathrm{I}}^{\mathrm{ss}}$ even though the craze length c decreases.

The fracture energy is affected in a more direct way by changing the critical craze opening $\Delta_{\mathrm{n}}^{\mathrm{c,cr}}$. This can be understood from the fracture energy $\phi_{\mathrm{n}} = \sigma_{\mathrm{c}} \Delta_{\mathrm{n}}^{\mathrm{c,cr}}$. In Fig. 11, the results for $\Delta_{\mathrm{n}}^{\mathrm{c,cr}} = 1.0 \times 10^{-3}$, 2.7×10^{-3} and 6.0×10^{-3} mm are shown for a constant loading rate $\dot{K}_{\mathrm{I}} = 0.1$ MPa mm$^{1/2}$ s^{-1}. Increasing $\Delta_{\mathrm{n}}^{\mathrm{c,cr}}$ directly increases the craze length because of the extended lifetime of the craze. As a result of this, the steady state fracture toughness $K_{\mathrm{I}}^{\mathrm{ss}}$ increases. For larger values of $\Delta_{\mathrm{n}}^{\mathrm{c,cr}}$, the steady state fracture toughness is better approximated by $K_{\mathrm{D}}^{\mathrm{ss}}$ (Fig. 11).

4.3. Parameter 3, E/σ_c

From the elastic displacement fields for mode I crack tip loading given in Eqs. (10) and (11), it is clear that for a constant loading rate $\dot{K}_{\mathrm{I}}$ and increasing Young's modulus E, the norm of the displacement rates $\dot{u}_1$ and $\dot{u}_2$ decreases. This also lowers the cohesive surface opening rate $\dot{\Delta}_{\mathrm{n}}$. The consequence of this is a lower drawing stress T_{n} because of which both the craze tip propagation speed and the life time of the fibrillar material increase. Consequently, the SIF for crack growth initiation K_{I}^0 increases for increasing Young's modulus E. Effectively, increasing the value of E/σ_{c} results in a more slender craze since the maximum separation of the craze–bulk interfaces $\Delta_{\mathrm{n}}^{\mathrm{c,cr}}$ is assumed to be constant. The larger craze length c results in a higher steady-state value $K_{\mathrm{I}}^{\mathrm{ss}}$ of the stress intensity factor.

In Fig. 12, the crack growth resistance curves for a loading rate of $\dot{K}_{\mathrm{I}} = 1.0$ MPa mm$^{1/2}$ s^{-1} are given. Note that the value of $K_{\mathrm{D}}^{\mathrm{ss}}$ increases from 8.1 MPa mm$^{1/2}$ for $E/\sigma_{\mathrm{c}} = 27$ to 32.4 MPa mm$^{1/2}$ for $E/\sigma_{\mathrm{c}} = 432$. The Dugdale estimate for the steady state value $K_{\mathrm{I}}^{\mathrm{ss}}$ of the stress intensity factor improves for increasing E/σ_{c}. The evolution of the craze length during crack growth is given in Fig. 13. The length of the plastic zone c_{D} increases from 0.029 mm for $E/\sigma_{\mathrm{c}} = 27$ to 0.46 mm for $E/\sigma_{\mathrm{c}} = 432$. The Dugdale estimate for the craze length becomes worse for increasing E/σ_{c}.

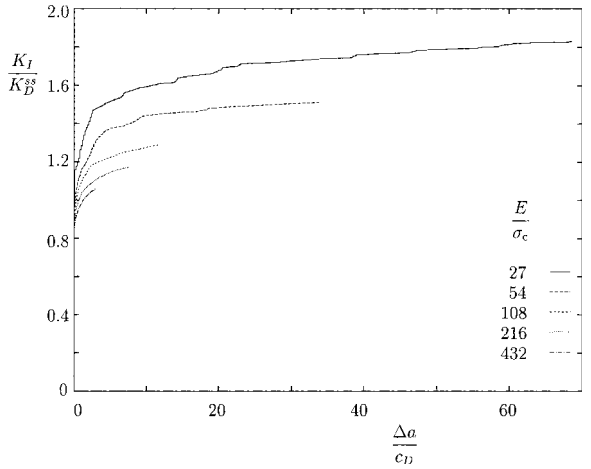

Fig. 12. Crack growth resistance curves for variation of E/σ_c.

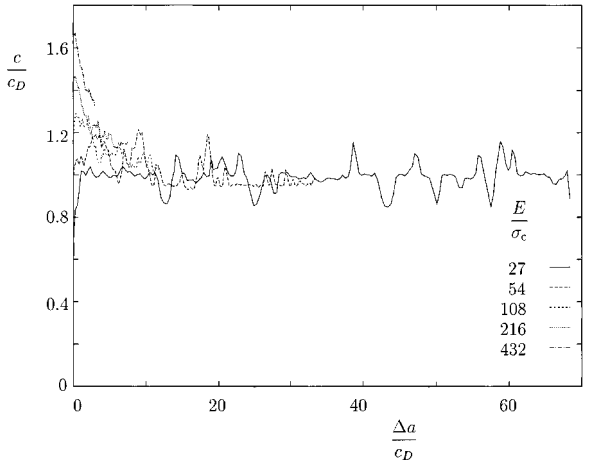

Fig. 13. Development of craze length c/c_D as a function of crack length $\Delta a/c_D$ for various E/σ_c.

5. Convergence aspects

Once crazing is initiated, further deformation tends to localize in the cohesive surface. Localization problems are known in general to exhibit a significant mesh dependency, but the sensitivity of embedded cohesive surface models as used here needs to be explored.

In their pioneering paper, Xu and Needleman (1994) applied the cohesive surface methodology to dynamic crack growth in brittle solids. Contrary to the present model designed for crazing, they used a phenomenological, elastic constitutive law for their cohesive surface. They reported calculations in which the orientation of the cohesive surfaces is varied and the influence on the crack growth direction is studied. Their results indicate that the cohesive surface orientation can have a significant influence on both the mode of crack growth and the crack growth speed. It is hard to conclude from the results of Xu and Needleman

(1994) whether crack growth convergence will occur upon further mesh refinement. This section therefore focuses specifically on convergence upon mesh refinement.

5.1. Symmetric versus asymmetric and unstructured meshes

The cohesive surface model for crazing relies on a craze initiation criterion to start the crazing process. Criterion (1) used in our model relates the cohesive normal traction T_n and the hydrostatic stress σ_m to a critical stress state. Apart from the cohesive surface element length, the orientation of cohesive surface elements will therefore have a significant influence on the craze path to be followed. For the mode I crack tip loading used in this paper, a mesh providing a horizontal row of cohesive surface elements in front of the initial crack tip gives the trivial solution of a horizontally propagating craze. The objective of the cohesive surface methodology, however, is to model the fracture behavior of solids without a priori assuming a crack path to be followed. The latter should be an outcome of the analysis.

If a horizontal row of cohesive surface elements in front of the crack tip does not exist, mesh refinement with structured meshes does not lead to the desired behavior. This is shown in Fig. 14. In Fig. 14a, the craze path and effective stress distribution are shown, as obtained with a relatively coarse mesh. Although the craze does propagate in the horizontal direction in some average sense, there is a clear tendency to meander. The craze deviates from its current path when a cohesive surface element is encountered with a more favorable direction. From Fig. 14b, it is seen that mesh refinement does not necessarily improve the situation.

Clearly, the orientation of the mesh determines the craze path to a large extent if structured meshes are used. To explore this further, we have constructed fully unstructured meshes by randomizing the mesh. Such a mesh should, upon mesh refinement, provide enough freedom for the craze to follow a 'correct' path. In Fig. 15, the propagation of a craze is shown for increasing values of the SIF. The propagation of the craze is a result of the competition between unloading of the bulk due to widening of existing crazes and the initiation of new crazes. A number of small craze branches are generated during propagation. The aforementioned competition in the end determines the ultimate path. Due to the random orientation of the cohesive surface elements, the craze is now better able to follow the horizontal path that is expected from symmetry.

5.2. Crack growth resistance curves

The energy needed for the crack to propagate is determined by the path that is chosen by the craze tip. Craze branching in amorphous polymers with an inhomogeneous microstructure may therefore increase the toughness. Lee et al. (1987) have shown experimentally that the increase in fracture toughness of many engineering polymers derives from the formation of multiple crazes at crack tips. In a fully unstructured mesh, the competition between various craze branches determines the final craze path and therefore may affect the predicted crack growth resistance.

In Fig. 16, a comparison is made between the crack growth resistance for the case in which the craze follows the ideal horizontal path by introducing only a single row of cohesive surface elements ahead of the crack (Section 4) and the case in which the craze must determine its path through a fully unstructured mesh. Upon mesh refinement, it is seen that an increase in crack growth resistance is achieved (roughly 5%). It was shown earlier that the fully unstructured meshes are capable of resolving an almost horizontal craze path so that the increase in crack growth resistance must be attributed to the many craze branches.

The crack growth resistance curve is influenced by the elastic stiffnesses k_α. Tijssens et al. (2000) pointed out that a cohesive surface should have an elastic stiffness that is much larger than the elastic stiffness of the surrounding continuum since otherwise the elastic properties of the combination of elastic continuum and cohesive surfaces do not accurately represent the original elastic properties of the continuum. In a one-dimensional setting, it is readily shown that the additional compliance due to cohesive surfaces of stiffness

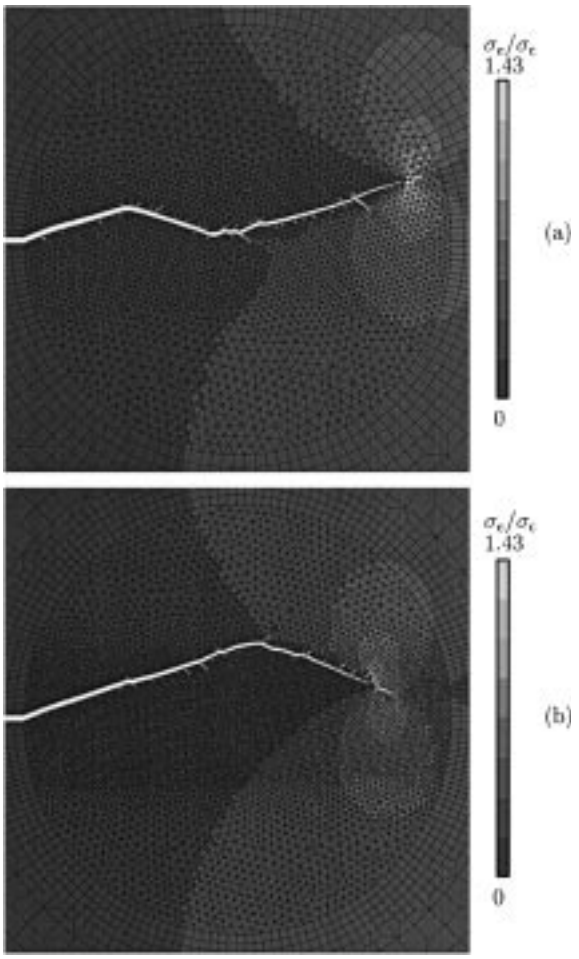

Fig. 14. Craze propagation and distribution of effective stress σ_e in (a) a coarse mesh and (b) a fine mesh in which still a clear structure exists.

k_n at a spacing l is of the order $E/(k_n l)$ relative to unity. This holds, approximately, also in a two-dimensional network with average mesh size l. Hence, as long as $E/(k_n l) \ll 1$, the additional elastic compliance due to the cohesive surfaces can be neglected. In Fig. 17, a comparison is made between the crack growth resistance curves for three meshes in which a craze is represented by 6, 12 or 24 cohesive surface elements. Only one row of cohesive surface elements in front of the crack tip is used, for which $E/(k_n l)$ is equal to 0.02 or 0.002. The elastic stiffnesses k_α in this paper are chosen without reference to experiments. It is evident from Fig. 17 that for too coarse meshes, the stiffnesses can still have a significant influence on the crack growth resistance even if $E/(k_n l)$ is small enough. However, we also observe that the influence of k_α diminishes when steady state crack growth is approached. The dependence of the crack growth resistance on the elastic stiffness k_α disappears when a single craze is represented by roughly 25 cohesive surface elements.

Warren et al. (1989) showed that the stress distribution around a craze is extremely sensitive to the precise opening profile of the craze. They argued that the stress field around a craze cannot be calculated from experimentally measured craze opening profiles using Fourier transform, boundary integral or finite

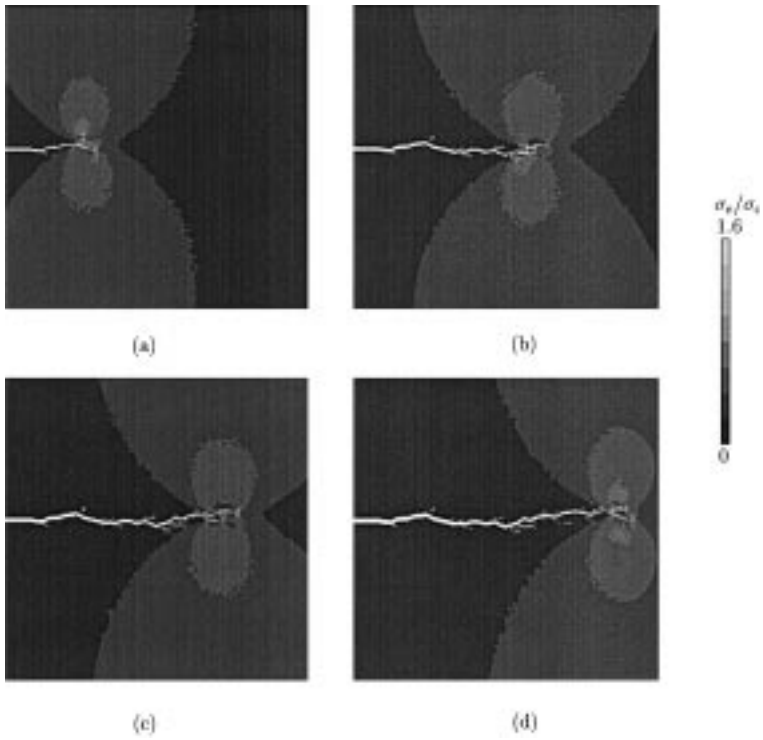

Fig. 15. Craze propagation and distribution of effective stress σ_e in an unstructured mesh. Material parameters are as stated in Table 1: (a) $K_I = 24.0$ MPa$\sqrt{\text{mm}}$, (b) $K_I = 26.1$ MPa $\sqrt{\text{mm}}$, (c) $K_I = 27.1$ MPa $\sqrt{\text{mm}}$ and (d) $K_I = 27.7$ MPa $\sqrt{\text{mm}}$.

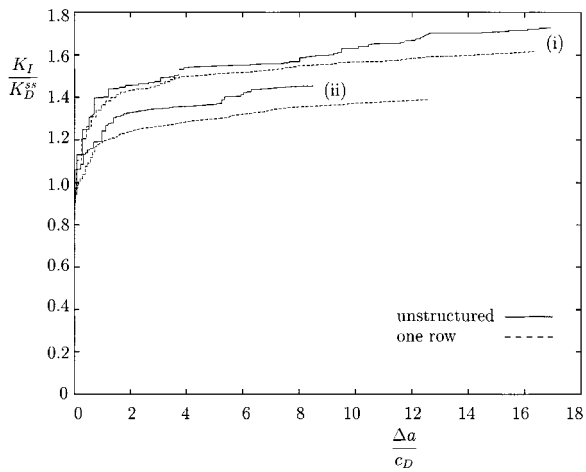

Fig. 16. Crack growth resistance curve for a fully unstructured mesh and for a single row of cohesive surface elements in front of the initial crack tip for (i) a coarse mesh and (ii) a fine mesh.

element techniques due to the boundary value problem being ill-conditioned. They showed that small errors, falling within the experimental tolerance, cause a significant change in the calculated stress field. No assumption on opening profiles is made in our calculations, and Fig. 18 clearly demonstrates that upon

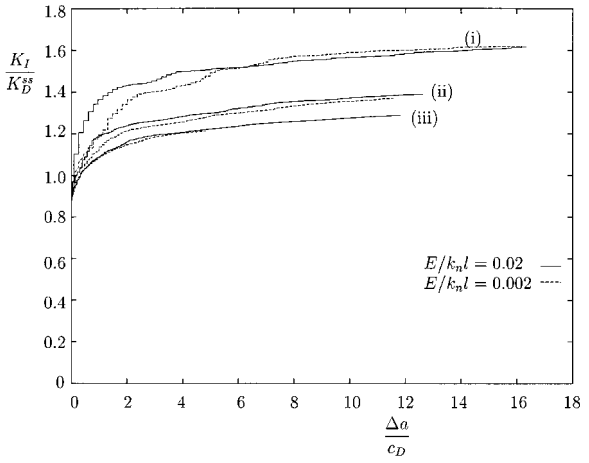

Fig. 17. Crack growth resistance curves for symmetric meshes with only one row of cohesive surfaces in front of the crack tip. Number of cohesive surface elements representing a craze equals (i) 6, (ii) 12 and (iii) 24.

mesh refinement the opening profile of the craze does not change significantly. However, the stress distribution in the neighborhood of the craze converges only for very fine meshes because of the traction gradients near the craze and crack tip. The stress distribution influences the crack growth resistance through the competition between crazing and unloading of the surrounding bulk. For an accurate description of the crack growth resistance, very fine meshes are therefore needed, as is shown in Fig. 17.

6. Effect of cross-tie fibrils

Crazes are known to have a complex structure in which long fibrils, spanning the gap between both bulk–craze interfaces, are interconnected by cross-tie fibrils. The cross-tie fibrils give the craze some tangential load carrying capacity. In Section 5, it was argued that a cohesive surface must not alter the initial elastic properties of the continuum too much and must therefore have a large (initial) stiffness. However, physically, a well-developed craze has a relatively low (but finite) tangential stiffness due to the presence of the cross-tie fibrils. The precise way in which the tangential stiffness evolves as the craze widens will depend on the mechanism that is responsible for creating cross-tie fibrils. Chain scission and disentanglement will certainly play a role (Kramer and Berger, 1990), but the precise kinetics are still unknown and detailed studies on craze widening such as in Van der Giessen and Lai (1997) are needed to provide this information.

The influence of the cross-tie fibrils reaches beyond the tangential load carrying capacity. Brown (1991) was the first to show the important role of the cross-tie fibrils in creating a stress concentration at the crack tip of a magnitude large enough to cause scission of molecular chains. Hui et al. (1992) and later Sha et al. (1997) further explored the role of the cross-tie fibrils with a detailed model of a craze. The description of crazing in a cohesive surface aims at a length scale at which the complex cross-tie fibril network of the craze is no longer visible. Only the capability of the craze to transmit traction from one bulk-craze interface to the other is captured in an effective traction–separation law. In a cohesive surface model, the role of the cross-tie fibrils in both the tangential load carrying capacity and the breakdown of the craze should therefore be incorporated through a dependence on the tangential separation Δ_t. This scale transition from the detailed craze structure to the cohesive surface length scale has not been made as yet. In order to understand the influence of cross-tie fibrils, we will briefly investigate the influence of the evolution of the tangential cohesive stiffness and the craze breakdown modeling on the predicted crack growth resistance curves.

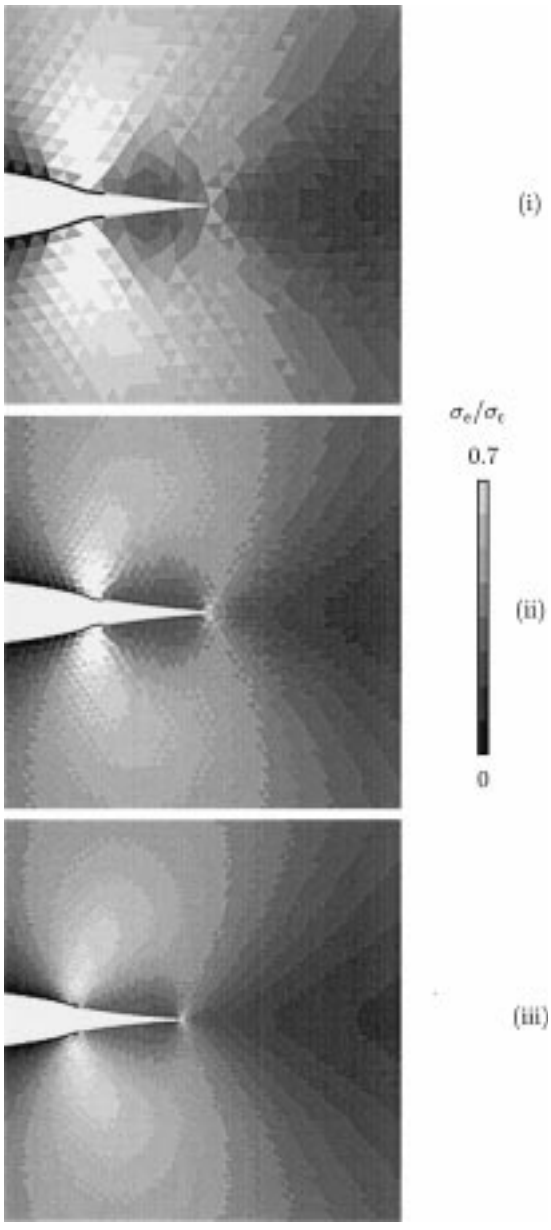

Fig. 18. Craze opening profiles and distribution of effective stress σ_e for progressively finer meshes and total crack extension $\Delta a/c_D \approx 7.5$ mm. Number of cohesive surface elements representing a craze equals (i) 6, (ii) 12 and (iii) 24, as in Fig. 17.

6.1. Tangential separation mode

The tangential stiffness evolution is described by Eq. (8). All previous calculations were performed with parameters $c_1 = 100$ and $c_2 = 0.3$. In Fig. 19, crack growth resistance curves are given for various values of c_1 and c_2. The value of c_1 determines the rate at which the stiffness k_t drops to zero, whereas c_2 determines for which value of the plastic normal separation, this drop occurs, as shown in Fig. 4. The result for a

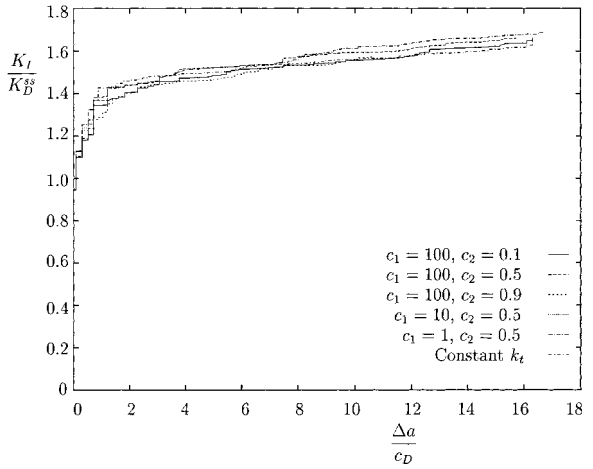

Fig. 19. Influence of the evolution of the tangential stiffness on the predicted crack growth resistance curve. Values of the parameters c_1 and c_2 in Eq. (8) as indicated are illustrated in Fig. 4.

constant tangential stiffness that only falls off as the craze breaks down is also shown in Fig. 19. The calculations were done with the fully unstructured mesh (i) in Fig. 16.

In Section 5.2, we showed that when using a fully unstructured mesh, craze branches can be captured that cause an increase in crack growth resistance of roughly 5%. When varying the constants c_1 and c_2 in Eq. (8), it is clear from Fig. 16 that the crack growth resistance curves are almost the same. The upper and lower curve deviate less then 5% from each other. This suggests that the precise way in which the tangential stiffness decreases with the plastic craze separation Δ_n^c does not dominate the solution.

6.2. Breakdown of crazes

In the cohesive surface model, a craze breaks down when a material dependent maximum separation of the craze-bulk interfaces has occurred (Section 2.1). The sudden breakdown of fibrils is captured in the model by a sudden loss of load carrying capacity in a cohesive surface integration point. For reasons of numerical stability, cohesive tractions T_α and stiffnesses k_α are decreased to zero in a predetermined number of increments. This rather crude description of craze breakdown may affect the outcome of the crack growth resistance curves in a quantitative sense.

In Fig. 20, the influence of the number of increments used to reach complete breakdown of the craze on the crack growth resistance curves is illustrated using results of calculations with a single cohesive surface laid out in front of the initial crack tip. Breakdown is taken to occur in a number of increments between 10 and 160. All previous calculations were performed with the number of increments in which full breakdown occurs set to 40. If craze breakdown is mainly governed by the presence of imperfections like dust-inclusions, immediate breakdown of the craze can be expected over a width of the same order of magnitude as the dimension of the imperfection. It is expected therefore that a better description of craze breakdown is obtained when the number of increments used to reach full breakdown is rather small, although this inevitably is related to the mesh density. The denser the mesh is, the better the numerical scheme captures the essential features of craze breakdown. From Fig. 20, it is clear that using too many increments results in a higher steady-state value of the mode I stress intensity factor due to the extended load-carrying capacity of the craze. For less then 40 increments, the resulting crack growth resistance is no longer significantly dependent on it anymore.

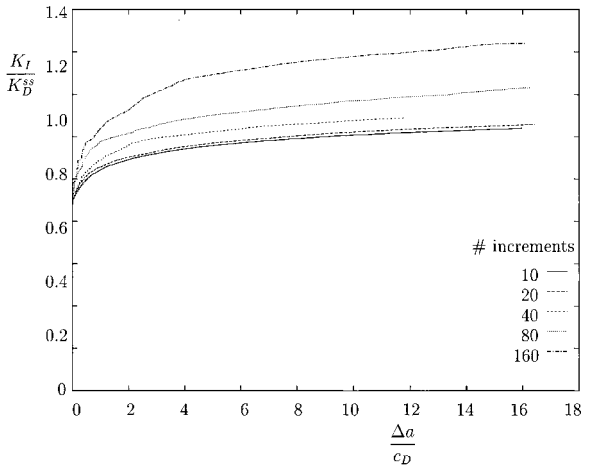

Fig. 20. Influence of the number of increments needed to reach full craze breakdown on the crack growth resistance.

7. Conclusion

Craze and crack propagation has been studied under mode I near-tip conditions using a recently proposed cohesive surface model for crazing in amorphous polymers. Crack growth resistance has been analyzed for a range of values of key material parameters.

For a constant loading rate, the crack growth resistance is found to diminish for relatively short crazes. This is consistent with the traditional Dugdale-like cohesive zone model which can be regarded as an ideal rate-independent craze. However, when the viscoplastic drawing process during craze widening becomes more important, a reversal of the previously noted trend can occur, i.e. a higher steady state mode I stress intensity factor despite a shorter craze length. This indicates that the Dugdale cohesive surface model cannot be used to describe crazing in these circumstances. Our calculations indicate that this is the case for temperatures around room temperature ($T = 293$ K) and loading rates higher then 0.1 $\mathrm{MPa\,mm^{1/2}\,s^{-1}}$ (lowest loading rate used in our calculations). Comparisons with experiments do not seem possible at this stage unfortunately. Experimental investigations often only report the value of the mode I SIF and rate dependency seems to be excluded a priori.

The cohesive surface methodology is shown to produce mesh independent results once the crazing process is resolved sufficiently accurate. Mesh orientation and density effects are important only if the orientation of cohesive surface elements is not statistically random. Upon mesh refinement, a correct craze path is obtained as a result of the competition between initiation of new crazes, the widening of existing crazes and the corresponding relaxation of the bulk.

References

Brown, H.R., 1991. A molecular interpretation of the toughness of glassy polymers. Macromolecules 24, 2752–2756.

Döll, W., Schinker, M.G., Könczöl, L., 1979. A time independent fracture criterion for PMMA. Int. J. Fract. 15, R145–R149.

Döll, W., Seidelmann, U., Könczöl, L., 1980. On the validity of the Dugdale model for craze zones at crack tips in PMMA. J. Mat. Sci. 15, 2389–2394.

Dugdale, D.S., 1960. Yielding of steel sheets containing slits. J. Mech. Phys. Solids 8, 100–104.

Estevez, R., Tijssens, M.G.A., Van der Giessen, E., 2000. Modeling of the competition between shear yielding and crazing in glassy polymers. J. Mech. Phys. Solids, submitted for publication.

Hui, C.Y., Ruina, A., Creton, C., Kramer, E.J., 1992. Micromechanics of crack growth into a craze in a polymer glass. Macromolecules 25, 3948–3955.

Kramer, E.J., 1983. Microscopic and molecular fundamentals of crazing. Adv. Polym. Sci. 52/53, 1–56.

Kramer, E.J., Berger, L.L., 1990. Fundamental processes of craze growth and fracture. Adv. Polym. Sci. 91/92, 1–68.

Lee, L.H., Mandell, J.F., McGarry, F.J., 1987. Fracture toughness and crack instability in tough polymers under plane strain conditions. Polym. Engng. Sci. 27, 1128–1136.

Leonov, A.I., Brown, H.R., 1992. A model of fibril deformation in crazes. J. Polym. Sci. B 29, 197–209.

Peirce, D., Shih, C.F., Needleman, A., 1984. A tangent modulus method for rate dependent solids. Comput. Struct. 18, 875–887.

Schellekens, J.C.J., De Borst, R., 1993. On the numerical integration of interface elements. Int. J. Num. Meth. Engng. 36, 43–66.

Sha, Y., Hui, C.Y., Ruina, A., Kramer, E.J., 1997. Detailed simulation of craze fibril failure at a crack tip in a glassy polymer. Acta Mat. 45, 3555–3563.

Sternstein, S.S., Ongchin, L., Silverman, A., 1968. Inhomogeneous Deformation and Yielding of Glasslike High Polymers. Appl. Polym. Symp. 7, 175–199.

Tijssens, M.G.A., Van der Giessen, E., Sluys, L.J., 2000. Modeling of crazing using a cohesive surface methodology. Mech. Mat. 32, 19–35.

Van der Giessen, E., Lai, J., 1997. A numerical study of craze growth. In: Deformation, Yield and Fracture of Polymers, vol. 10. The Institute of Materials, London, pp. 35–38.

Warren, W.E., Chudnovsky, A., Mullen, R.L., 1989. On the accuracy of the calculated stress field around a craze. Polym. Engng. Sci. 29, 426–431.

Xiao, F., Curtin, W.A., 1995. Numerical investigation of polymer craze growth and fracture. Macromolecules 28, 1654–1660.

Xu, X.-P., Needleman, A., 1994. Numerical simulations of fast crack growth in brittle solids. J. Mech. Phys. Solids 42, 1397–1434.